Effect of unbalanced topography and overloading on Coulomb wedge kinematics: Insights from sandbox modeling

Mario Del Castello
Istituto di Scienze Marine-Consiglio Nazionale delle Ricerche, Sezione di Geologia Marina, Bologna, Italy

Gian Andrea Pini
Dipartimento di Scienze della Terra e Geologico Ambientali, Università di Bologna, Bologna, Italy

Kenneth R. McClay
Fault Dynamics Research Group, Department of Geology, Royal Holloway, University of London, London, UK

Received 30 July 2003; revised 3 March 2004; accepted 1 April 2004; published 20 May 2004.

[1] This study addresses the effect of variable unbalanced topography and overload on the kinematics of a fold and thrust belt developed within a collisional belt that underwent a subduction polarity reversal event. This was done by physical modeling of doubly vergent Coulomb wedges, using sand as an analogue material. During the experimental procedure a preexisting topography was generated by a first phase of subduction in one direction. A second phase of subduction was then initiated in the opposite direction (simulating a subduction flip). An anomalous, strong frontal growth for the wedge during the second phase was experimentally shown to be dependent upon surface slope breaks and the critical asymmetrical architecture achieved by the wedge at mature stages of deformation. The latter is suggested to be the rule for doubly vergent orogens at steady state, even after a subduction flip. During the experiments, surface processes, like syntectonic erosion and sedimentation, markedly altered mass transfer within the wedge. In particular, lowering the surface slope by syntectonic erosion favored cycling between accretion and underthrusting modes. By contrast, a sudden syntectonic sediment load in the prowedge region promoted prolonged phases of underthrusting, retarding accretion of new imbricates at the prowedge toe. However, at later stages of deformation the prowedge was forced to regain its characteristic minimum critical taper as predicted by theory and did so by the sudden nucleation of long, flat thrust units, rapidly rebalancing the asymmetry between prowedge and retrowedge regions. The experiments suggest that given a fixed critical taper related to time-invariant frictional properties along the wedge bounding surfaces, deformation does vary within the wedge according to time-varying location of normal stress surpluses and unbalanced topography acting on potential failure surfaces. These, in turn, alter the equilibrium between prowedge and retrowedge basal detachments that is here considered to be a major factor controlling the self-regulating dynamics of collisional orogens. *INDEX TERMS:* 8020 Structural Geology: Mechanics; 8102 Tectonophysics: Continental contractional orogenic belts; 8168 Tectonophysics: Stresses—general; *KEYWORDS:* sandbox modeling, wedge kinematics, unbalanced topography

Citation: Del Castello, M., G. A. Pini, and K. R. McClay (2004), Effect of unbalanced topography and overloading on Coulomb wedge kinematics: Insights from sandbox modeling, *J. Geophys. Res.*, *109*, B05405, doi:10.1029/2003JB002709.

1. Introduction

[2] Mechanical and kinematic controls exerted on fold and thrust belt evolution by pure frictional rheology along potential failure surfaces have been widely applied to model compressional systems in nature. The idea that the architecture of thrust systems resembles that of a wedge of noncohesive material deforming ahead of an advancing bulldozer has led to exploring the mechanics of wedges deforming at convergent margins according to the Coulomb theory. Two- and three-dimensional theoretical treatments [*Chapple*, 1978; *Dahlen*, 1984; *McCaffrey*, 1992; *Platt*, 1993], numerical analyses [*Willett et al.*, 1993; *Braun and Beaumont*, 1995; *Burbidge and Braun*, 2002], and physical approaches [e.g., *Malavieille*, 1984; *Marshak and Wilkerson*, 1992; *Pinet and Cobbold*, 1992; *Koons*, 1990; *Wang and Davis*, 1996; *Burbidge and Braun*, 1998; *Storti et al.*, 2000] incorporate the Mohr-Coulomb failure criterion to various degrees. This approach is fundamentally justified by labo-

0148-0227/04/2003JB002709$09.00

ratory experiments, suggesting that rock deformation obeys the Coulomb failure criterion to good approximation under pressures and temperatures characteristic of the upper crustal levels [*Byerlee*, 1978]. Initially applied to accretionary complexes, the critical wedge theory has been extended to entire collisional orogens on the basis of the "orogenic wedge" hypothesis [*Platt*, 1986] which predicts that gravitational forces (surface slope) and basal shear tractions (subduction controlled) to balance each other at crustal scale until the orogen achieves a steady state configuration. However, this simple model does not take into account rheological variations at the crustal scale (e.g., deformation behavior of upper versus lower crust).

[3] Modern studies of orogen dynamics have provided great insights into the influence of factors, which control the temporal evolution of mountain ranges, other than plate motion alone. From a dynamic perspective, the increase in elevation is a process by which an orogen progressively stocks up potential energy that can be dissipated through time, giving way to a series of geologic scenarios impossible to predict from plate tectonics principles alone. This new approach attempts to explain how dynamic mechanisms affecting the spatial and temporal feedback between growing topography and surface processes, such as erosion and sedimentation, may overprint first-order, large-scale orogen geometries generally thought to derive primarily from lithospheric plate interactions. Excess topography developed across collisional orogens and its gravity effect have been invoked to explain unbalanced states of compression in the crust [*England and Molnar*, 1997] and strong phases of reactivation for large-scale thrusts [*Hodges et al.*, 2001; *Wobus et al.*, 2003]. On the other hand, the proposed explanation of orogen mechanics by means of critical wedge theory assigns major importance to how orogen mass is continuously removed from elevated areas and redistributed toward depressed regions, for this perturbs the balance between gravitational stresses within the accreting system and basal shear stresses resulting at the subduction interface. The steady state condition, implied by the self-similar growth characteristic of the Coulomb wedge model, may not always be applicable when surface processes drive large-scale mass redistribution across the mountain range [*Willett*, 1999b].

[4] This paper addresses the problem of the effect of excess topography and unbalanced overload developed at those particular convergent margins for which subduction polarity reversal has occurred. This process was investigated as a possible mechanism to produce preexisting topography and overload over a broad region. We tested whether critical wedge theory can provide an explanation for possibly anomalous wedge behavior after the subduction polarity "flip" event.

2. Topography and Subduction Polarity Reversal

[5] Although proposed as an explanation for the tectonic evolution of many collisional orogens, subduction polarity reversal remains a controversial yet intriguing topic of debate. A subduction polarity flip event has been invoked in all those cases where the peculiar metamorphic-tectono-stratigraphic signal and/or the lack of peculiar tectonic domains could not be interpreted by means of a single subduction zone with constant (unidirectional) vergence. These include the Caribbean Arc [*Lebron and Perfit*, 1994; *Draper et al.*, 1996; *Smith et al.*, 1999], the Banda Arc [*Snyder et al.*, 1996], the Borneo suture [*Hall and Wilson*, 2000], Taiwan [*Chemenda et al.*, 2001; *Carena et al.*, 2002], and the Kamchatka Arc [*Konstantinovskaya*, 2001]. For such settings, one explanation offered was a subduction flip aided by the involvement of a thinned overriding crust in the subduction zone, due to the presence of volcanic arc-related crustal weakening, and the interplay between upper plate flexural rigidity and thickness and interplate friction [*Tang and Chemenda*, 2000]. At the same time, subduction polarity reversal has also been postulated for full continent-continent collision as in the case of the Apennines [*Elter and Marroni*, 1991; *Castellarin*, 1994; *Doglioni et al.*, 1999] or the Himalayas [*Willett and Beaumont*, 1994; *DeCelles et al.*, 2002]. In this case, subduction polarity reversal should be the extreme consequence of a continuous process previously known as ablative subduction [*Tao and O'Connell*, 1992; *Pope and Willett*, 1998], whereby the lower crust pertaining to the overriding plate is progressively delaminated from the upper crust, leading to final inversion of the subduction direction.

[6] This peculiar case makes sandbox modeling particularly well suited for reproducing orogen mechanics, as deformation is restricted to the upper crust. We chose sandbox modeling of doubly vergent Coulomb wedges, as they better reproduce the overall structure of orogens observed at collisional margins [*Koons*, 1990; *Willett et al.*, 1993; *Beaumont et al.*, 2000; *Pfiffner et al.*, 2000]. In our case, excess relief and overload are essentially caused by the first phase of the contraction-inherited retrowedge region. This assumption corresponds well to the geometry of continental collision orogens imaged by deep seismic profiles, such as the Alps [*Schmid et al.*, 1996; *TRANSALP Working Group*, 2002] or the Pyrenees [*Choukroune and The ECORS Team*, 1989; *Daigniéres and The ECORS Team*, 1994; *Pulgar and ESCIN Group*, 1996]. These show how the overriding plate is bent under the weight of the retrowedge and related retrowedge foreland basin. At this stage, a hypothetical subduction flip would give way to the formation of a new thrust system characterized by an inherited unbalanced topographical aspect and vertical overload acting on potential detachment surfaces.

3. Experimental Method

[7] To estimate accretionary flux within the prowedge region when preexisting topography loads the shortening sedimentary (or rock) section, the shortening direction was inverted at a certain stage during wedge development. It follows that two distinct phases of contraction are produced (Figure 1) and the retrowedge related to the first phase of contraction rests on and overburdens the sand pack that will undergo deformation during the second phase (Figure 1b). In this manner, it is possible to study in detail how deformation is absorbed within the prowedge when previously built topography alters the overall internal state of stress with respect to a given internal/basal coefficient of friction ratio, as well as the relationships between two superposed and interfering thrust systems. This approach offers some advantages over previous studies: (1) the

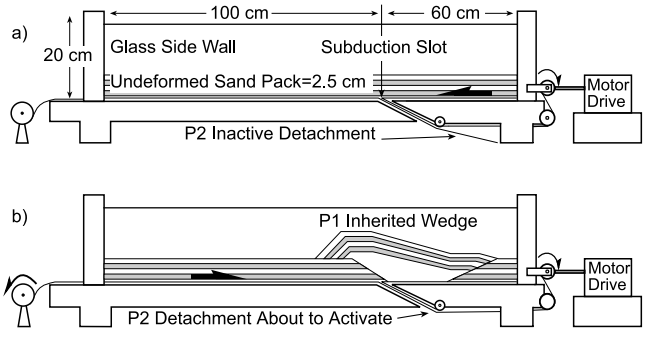

Figure 1. Schematic diagram of the deformation apparatus. (a) Beginning of first phase of shortening (P1). (b) End of P1, beginning of second phase of shortening (P2). The existing wedge belongs to P1. Black arrows indicate subduction vectors at the beginning of either phase.

overall wedge morphology inherited (i.e., size, taper angle), can be directly determined by the amount of shortening set up for the first phase; (2) in this way a nonrigid backstop builds up, keeping rheological properties unaltered, and the wedge itself is "free" to choose the most suitable backstop geometry according to its dynamic equilibrium; and (3) the system is closed (in terms of mass balance) and therefore there is a continuous feedback between mass transfer within the wedge (thrust sequences) and wedge attitude at the surface (variation of taper angle). Modifications of the initial set up were planned to analyze the effect of several variables on wedge development: syntectonic denudation, syntectonic sedimentation and addition of rheological weaknesses in the mechanical stratigraphy.

[8] The analogue experiments were performed in a glass-sided, rectangular deformation apparatus measuring 160 × 30 × 20 (L × W × H, in cm) internally (Figure 1a). The glass was carefully cleaned and coated by a friction-reducing transparent compound to minimize sidewall friction and allows an optimal recording of deformation increments by serial photographs. A strain singularity [*Willett et al.*, 1993] was produced by a subduction slot, where the basal detachment sheet (Mylar drafting film) is able to move, being dragged down by a motor-driven pulley. The two phases of contraction (P1 and P2, respectively) were obtained using two oppositely moving drafting sheets, passing through the same slot and sequentially pulled by the same roller (Figure 1). However, pretension was carefully applied to avoid affecting the sand pack during detachment sheet interchanging between the two phases.

[9] A homogeneous 2.5-cm-thick sand pack was constructed by a manual-layering machine, trying to minimize local inhomogeneities and packing anisotropy. The scaling factor is 10^{-5}, which means 1 cm of sand represents 1 km in nature [*McClay*, 1990; *Liu et al.*, 1992]. Moderately well rounded, well-sorted dry quartz sand (average grain size of 90–110 μm) was the material used to simulate the deforming brittle upper crust. The average grain diameter was smaller than that used in previous experiments [*Liu et al.*, 1992], for which laboratory tests indicate an internal friction angle varying between 31° and 42° according to the range of confining pressures (1300–1800 Pa and 160–400 Pa, respectively) [*McClay*, 1990, also unpublished Fault Dynamics Research Group Report, 1992]. Nevertheless, recent studies [*Schellart*, 2000] suggest that the coefficient of internal friction is mainly dependent on the sphericity of individual grains rather than on grain size, justifying the assumption of the same properties for the material adopted. Both faulted and unfaulted sand displays a linear Mohr failure envelope with a coefficient of friction of $\mu = 0.50$ and $\mu = 0.55$, respectively. The drafting film used to simulate the basal detachment was characterized by a $\mu_b = 0.47$ [*Liu et al.*, 1992]. Deformation was recorded using time lapse 35-mm photography every 0.5 cm deformation increment. Using a graphic software package, a set of parameters was systematically measured at 2-cm intervals to describe the evolution of the wedge. For each experiment, measurements were restricted to P2 only and compared to the wedge growth during P1. In fact, given the high degree of reproducibility for this set of models, P1 was measured for the first experiment only. The parameters measured were (Figure 2): displacement along each thrust ramp (D_n), maximum height reached by the axial zone (H), wedge toe outer location for both prowedge and retrowedge (L_p and L_r, respectively), and displacement for the axial zone bounding faults (D_p and D_r). Cumulative displacement for each thrust fault was plotted against a shortening ratio, expressed in terms of

$$S = L_f / L_i,$$

where L_f is progressive shortening applied to the sand pack and L_i is initial sand pack length.

[10] Because of deformation apparatus dimensions, for which the P2 undeformed sand pack was 100 cm long (refer to Figure 1), the shortening ratio coincides in value with the amount of shortening applied in the description of all the experiments. Measurements covered a shortening interval of 38 cm (~40% of shortening). This limit was set on the basis that P2 prowedge in the first experiment had already reached the minimum critical taper (~10°) characteristic of the sand used for these models. Moreover, this value is similar to the maximum shortening permitted for P1, allowing a direct comparison between the two phases.

4. Experimental Results

4.1. Basic Setup (CC-36)

[11] For the first experiment, the sand pack was shortened without modifying other experimental parameters during the wedge development. Therefore it was regarded as a template for subsequent model runs, and their results will be compared to this experiment. This section describes the main kinematic differences between P2 and P1 (see Figure 3 for immediate visualization) to be used as a reference point for later discussion.

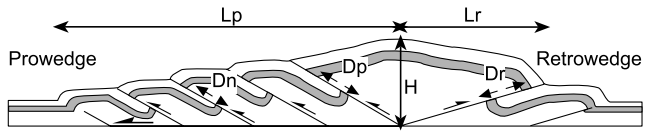

Figure 2. Reference framework of parameters measured for displacement curves.

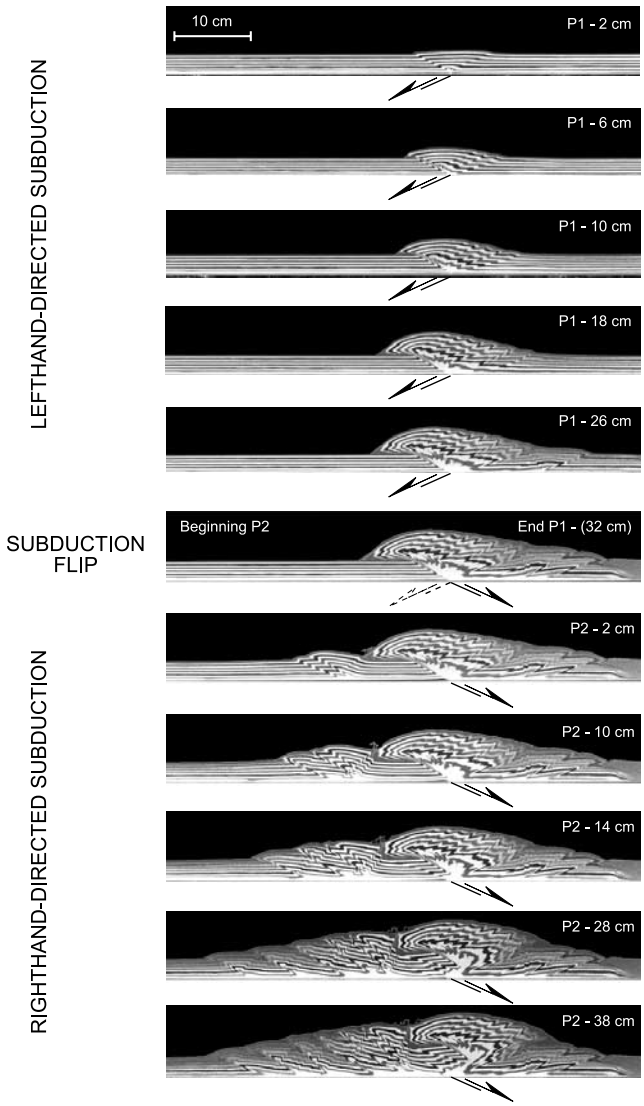

Figure 3. Basic differences of wedge kinematics between P1 and P2. Axial zone vertical uplift and later forward growth during P1 is replaced by dominant prowedge accretion and nearly zero uplift since early stage of P2. Black arrows indicate subduction vectors.

[12] After deforming the wedge during P1 up to the maximum contraction value permitted by the deformation rig, the inherited wedge architecture was characterized by a retrowedge extending to 10 cm away from the subduction slot (Figure 4a, stage I) at the maximum taper possible (sand angle of repose). At 1% of shortening, a detachment propagated at the base of the P2 prowedge, stepping the deformation front outward, far away from the subduction slot (17 cm). An asymmetric, foreland-verging anticline nucleated where the detachment ramped up through the sand pack, with a nearly simultaneous retrovergent kink band pointing toward the P1 retrowedge toe (Figure 4a, stage II). P2 prowedge growth showed rapid accretion of new frontal imbricates from an advanced strain discontinuity (Figure 4a, stage III), with a decreasing rate of thrust nucleation as deformation proceeded. The thrusts showed intermediate to long décollements and the associated anticline forelimb emerged at the surface with a constant distance from the prowedge toe (ranging between 5 and 6 cm). At about 14% of shortening (Figure 4a, stage IV), a first out-of-sequence small thrust nucleated at the subduction slot beneath the P1 retrowedge area. It was followed by similar structures at 23% and 28% of shortening. These, coupled with a prominent backthrust at the toe of the P1 retrowedge, determined the continuous vertical uplift of the axial region toward the final taper surface (Figure 4a, stage V). Toward the end of the model run (≈40% of shortening), the minimum critical taper had already been achieved in the P2 prowedge (Figure 4a, stage VI). The topography in the P2 retrowedge area displayed a higher taper than in the prowedge approximating a maximum critical taper and indicating that the theoretical morphology of a doubly vergent wedge is respected even when such a complex subduction evolution is applied.

[13] A quantitative insight into wedge kinematics is given by displacement curves (Figure 4b). The first two thrust ramps (D1 and D2) were marked by a short period of activity, soon after which they reached an asymptotic value of maximum displacement of 0.75 and 0.95 cm, respectively. However, D2 underwent a distinct reactivation around 28% of shortening. The nucleation of the subsequent two thrusts (D3 and D4) displayed the same trend, but this time they were more longer lasting and displacement rates were higher during early stages (gradient nearly doubled). D4 accumulated the highest displacement, reaching a 3.86 cm value after a reactivation in out of sequence (32% of shortening). D5 and D6 showed equally high initial displacement rates in their early stages of deformation, but they died out rapidly, while D4 was still active in the inner part of the wedge. The measurement interval for D7 was too short to thoroughly characterize its kinematics but it showed the same high value of initial displacement rate as in D3, D4, D5, and D6. A detailed analysis of the displacement curves reveals that a transition might exist from piggyback to mixed piggyback and synchronous and, finally, to fully synchronous thrusting sequence toward the end of the model run (D2, D4, and D6 were active at the same time between 28% and 34% of shortening). Concerning the prowedge toe position in time, a continuous outward growth was observed at early stages of deformation (Figure 4c). This was due to nucleation of small-scale thrusts paralleled by scarce activity along the P2 retrothrust during the same displacement interval. This became more evident around 10% of shortening, promptly followed by a well-defined retreat of progressively new accreted imbricates (saw-tooth curve pattern), together with uplift of the axial zone (albeit small).

[14] In our experiments, the first stage during P1 corresponded to a rapid, symmetrical uplift, centered above the subduction slot (see Figure 3). The wedge grew in the form of a symmetric flat-topped pop-up structure, bounded at the rear by a very active retrothrust (future retrowedge region), whereas a set of high-frequency kink bands developed above the prothrust (future prowedge region). As Figure 4d shows, the axial zone uplift (H) was strong, as was the backward retrowedge growth (L_r). The gradient of prowedge growth (L_p) nearly equals L_r between 0% and 20–24% of shortening, confirming similar kinematics for prowedge and retrowedge

at this stage. Toward the final stages of shortening (44–64%), the wedge toe propagated very quickly, driven by a long detachment developed at the base of the prowedge, with the deformation front instantaneously stepping well ahead in the undeformed sand pack. Each frontal anticline was marked by a prolonged phase of retreat before nucleation of a new thrust. It is noteworthy that the retrothrust was still very active (D_r, Figure 4d), whereas retrowedge toe growth started to slow down at late stages of contraction (L_r, Figure 4e). This difference in motion was perhaps absorbed within the retrowedge region, during its rotation and reaching of the final maximum taper.

4.2. Kinematics Versus Syntectonic Denudation (CC-38)

[15] In this experiment, syntectonic denudation was introduced in two distinct stages during P2. Both the events reduced the surface slope to 10° (minimum taper for this sand) in different parts of the wedge. The first rapid denudation event affected the P1 retrowedge region, to evaluate the impact of a lowered topography on P2 deformation, the width of the overburden being fixed. The second erosion event was instigated later, on the P2 retrowedge, to test whether this wedge region was able to increase its strain rate at a stage when it should already have been very active and if this inhibited deformation in the prowedge sector at the same time.

[16] The wedge dimensions at the beginning of the P2 were as in CC-36 (Figure 5a, stage I) and, as in that case, a foreland verging anticline propagated at the tip of a very long detachment in the prowedge region at the onset of P2. Conversely, in this model, no retrovergent kink band developed at the anticline back limb, this being true also at later stages of deformation (Figure 5a, stages II and III). The first thrust was followed by nucleation of a new ramp after 5% shortening. Following the first denudation event (operated at 10% shortening; Figure 5a, stage II), rapid prowedge accretion characterized this phase as in the

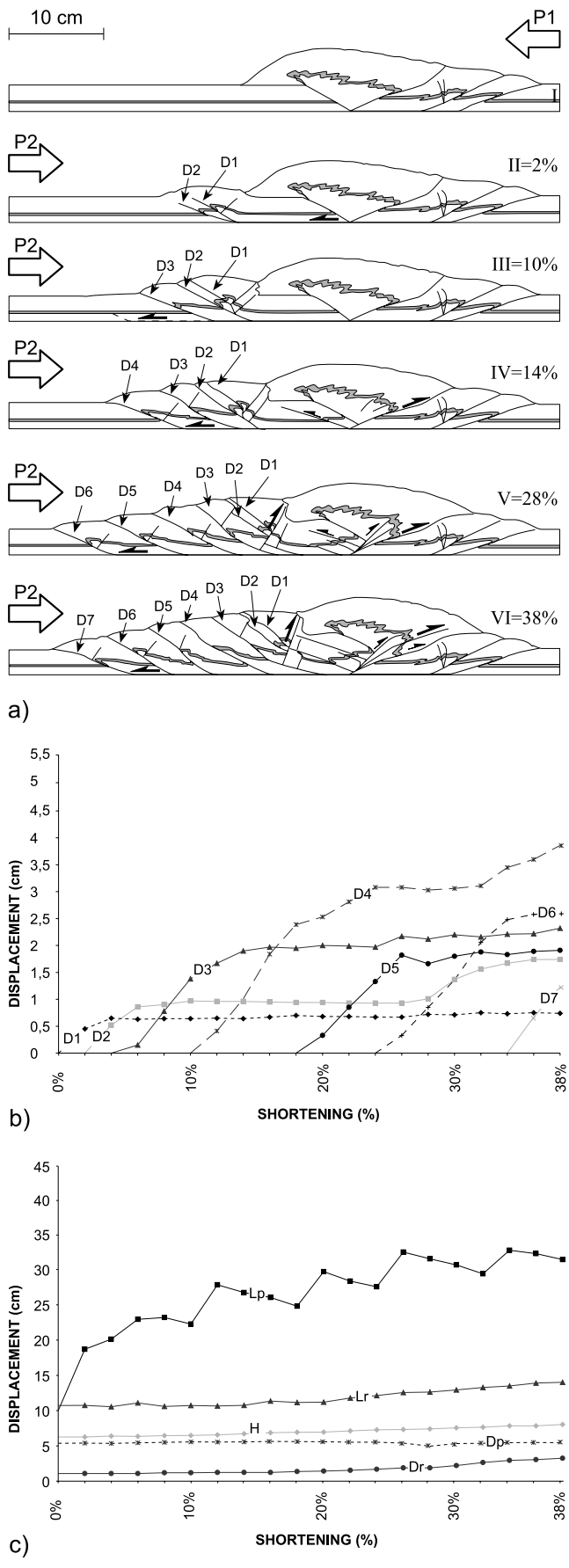

Figure 4. (a) Line drawings of sequential stages of wedge development during the second phase (P2) for experiment CC-36. Stage I is end of the first phase (P1). Different arrow sizes indicate dominant and secondary motion on thrust faults. (b) Displacement curves for each prowedge thrust (D1 to D7). (c) Distance of the wedge toes from the subduction slot: prowedge (L_p) and retrowedge (L_r). H is the axial zone maximum height and displacement for the axial zone bounding faults is marked by D_p and D_r (on the prowedge and retrowedge sides, respectively). Because of 100 cm initial undeformed length, percent of shortening equates to centimeters of shortening. (d) Progressive evolution of selected parameters of CC-36 experiment wedge growth during P1 (first phase) with displacement curves for the most long-lived thrusts in the prowedge. Note the reduced cumulative displacement on each fault and how the retrothrust (D_r) outpaces prowedge imbricates. (e) L_p showing the three evolutionary stages, from pop-up structure to fully developed doubly vergent wedge. Note larger shortening ratio required to achieve the wedge critical taper.

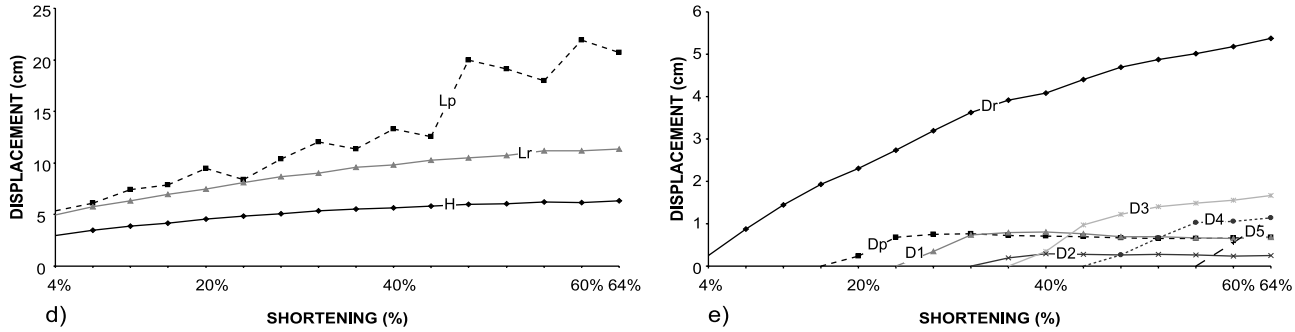

Figure 4. (continued)

previous experiment. However, a marked change in the wedge mass transfer took place. The third thrust unit accreted in the prowedge started to be passively underthrust, as seen by the related retrovergent kink band being progressively buried underneath the second imbricate (Figure 5a, stages III to V). The prowedge basal décollement must have exhibited complex mechanics at this stage. An active segment must be inferred in its outmost sector, where a new forethrust was propagating, but this was followed inward by a deactivated portion, which allowed the third thrust to be transported backward. At the same time, the basal detachment in the innermost sector had stepped up to a shallower position in the deforming section. Accordingly, the second anticline became unrooted from its ramp, the latter being dragged back toward the subduction slot (Figure 5a, stage V). The second erosional event did not strongly alter the deformation pattern in the P2 prowedge. In addition, it was very difficult to visibly define a distinct increase in strain rate in the P2 retrowedge. Toward the end of the model run, a new underthrusting cycle was possibly occurring in the prowedge outer region, where the fourth thrust started to branch through the outer anticline. This is clearly indicated by the asymmetric bulge in the fifth anticline hinge area (Figure 5a, stage VI).

[17] The D1 and D2 early stages of deformation were marked by high displacement rates, but for both faults there was a subsequent decline of activity (Figure 5b). The decreasing trend is less evident for D2, perhaps because the quiescence phase is inhibited by the first denudation event (10% of shortening). A strong out-of-sequence reactivation for D1 appeared much later (around 18% of shortening). This is interpreted as the décollement shallowing up (as previously described). During the shortening interval ranging between 18% and 22% of shortening, D1 was capable to regain the displacement difference with D2. They later deformed at comparable strain rates, meaning that the two imbricates were now growing on the same décollement (D1 plus D2). During the same deformation interval, D3 reached its quiescence asymptotic value and the difference in displacement with D1 plus D2 continuously increased till the end of the measured shortening interval (underthrusting beneath D1 plus D2). A piggyback thrusting sequence can be inferred from the plot for D4, D5, and D6 accretion following the underthrusting event. The effect of the second denudation event is not clear. It does not seem to alter thrust nucleation (only D6 is possibly triggered early) and strain rates in the prowedge (D3, D4, D5, D6) are comparable with other experiments. Even the P2 retrowedge region does not appear to be affected by this event (Figure 5c). The first erosional event shows a major effect (Figure 5c) marking the beginning of P2 retrowedge growth, coupled with a linear increase in wedge maximum height. Moreover, the decreased vertical load promoted a short-lived reactivation for the fault (D_p) bounding the base of the axial zone on the prowedge side.

4.3. Kinematics Versus Weaknesses in Mechanical Stratigraphy (CC-39)

[18] With this experiment, rheological anisotropies in the mechanical stratigraphy were modeled, with leveling glass beads into two different horizons. The first was layered at the base of the sand pack, thereby simulating a weaker basal décollement. The second layer was positioned closer to the surface, representing a shallower potential detachment. The glass beads were carefully layered in the P2 deformation sector only, so that they were located beyond the P1 retrothrust tip propagation domain. In other words, the presence of the mechanical anisotropy should theoretically not influence P1. Therefore its boundary conditions remained unaltered compared to previous experiments.

[19] The P2 initial setting shows a P1 retrowedge characterized by a width of 13.2 cm, the maximum observed during the experimental program. Coupled with a reduced P1 retrowedge height, this gives a lower taper inherited from the first phase of contraction in comparison to other experiments. The difference in P1 retrowedge width was due to a set of small-scale detachment folds developed at the foot of the advancing retrowedge main body (Figure 6a, stage I). A weak mechanical anisotropy (glass beads) in the footwall of P1 retrowedge caused some of the prowedge contraction to be absorbed in the stationary area where these small-scale folds were produced. Each small fold had a concomitant counterpart in the P1 prowedge suggesting that the propagation of a new thrust in the prowedge was accompanied by a backward translation of the wedge as a whole. As no fault is visible beneath the small-scale features, an active push exerted by the retrowedge on the horizontal glass beads detachment is believed to be responsible for the deformation. Moreover, detachment fold activity increased after 12–13% of shortening. This indicates that this stage is critical when wedge development passes from axial zone nearly vertical uplift to effective wedge backward displacement. The first thrust unit nucleated at 0.5% of shortening (Figure 6a, stage II), displaying a very

broad flat segment, longer than the corresponding units in previous experiments. However, the spacing between the thrust tip and the P1 retrowedge toe was similar. The position where the décollement ramped up through the sand pack was always located along the prolongation of the P1 retrowedge slope. As deformation progressed, relatively long décollement segments were activated sequentially at the prowedge toe, each of which showed a flat-topped box-fold at its tip (Figure 6a, stage III). The two glass bead layers provided the rheological weakness to produce a rapid forward growing P2 prowedge (the lowermost) and well-defined staircase trajectories for each thrust (the uppermost). The combined effect caused a rapid propagation of the deformation front, that coupled with the low topography of each imbricate, led to the critical minimum taper at very early deformation stages (less than 25% of shortening; Figure 6a, stage IV). Moreover, the presence of a second detachment in the uppermost part of the sand-pack favored continuing slip between units (as testified by the displacement of retrovergent kink band hinges), and efficient out-of-sequence thrusting beneath the P1 retrowedge region (Figures 6a, stages V and VI).

[20] The case with rheological anisotropies in mechanical stratigraphy showed a set of forward propagating faults, marked by prolonged activity throughout the deformation history (Figure 6b). Because of the basal weaker detachment, the initial fault growth occurred at the fastest rate observed in these experiments. However, despite the continuous displacement along each fault, an overall piggyback thrusting sequence can be inferred by displacement curves shape. In CC-39, it is difficult to distinguish a distinct reactivation on single fault planes. Rotation of imbricates causes progressive alignment between thrust ramps at depth and weak décollement at the surface. The latter activates very easily, ensuring ample layer-parallel thrusting at late deformation stages that mimics synchronous thrusting. The D2 thrust ramp may be the only one that undergoes out-of-sequence motion, as demonstrated by a cumulative displacement much higher than D1.

[21] The P2 prowedge toe position (Figure 6c) gives an idea of the high rate of outward stepping ahead for the deformation front. At 12% of shortening, the P2 prowedge width is already comparable to that observed toward the end of the model run for previous experiments. At early stages of contraction, the P2 prowedge region showed minimal toe retreat: only at 20% of shortening, when the P2 retrothrust

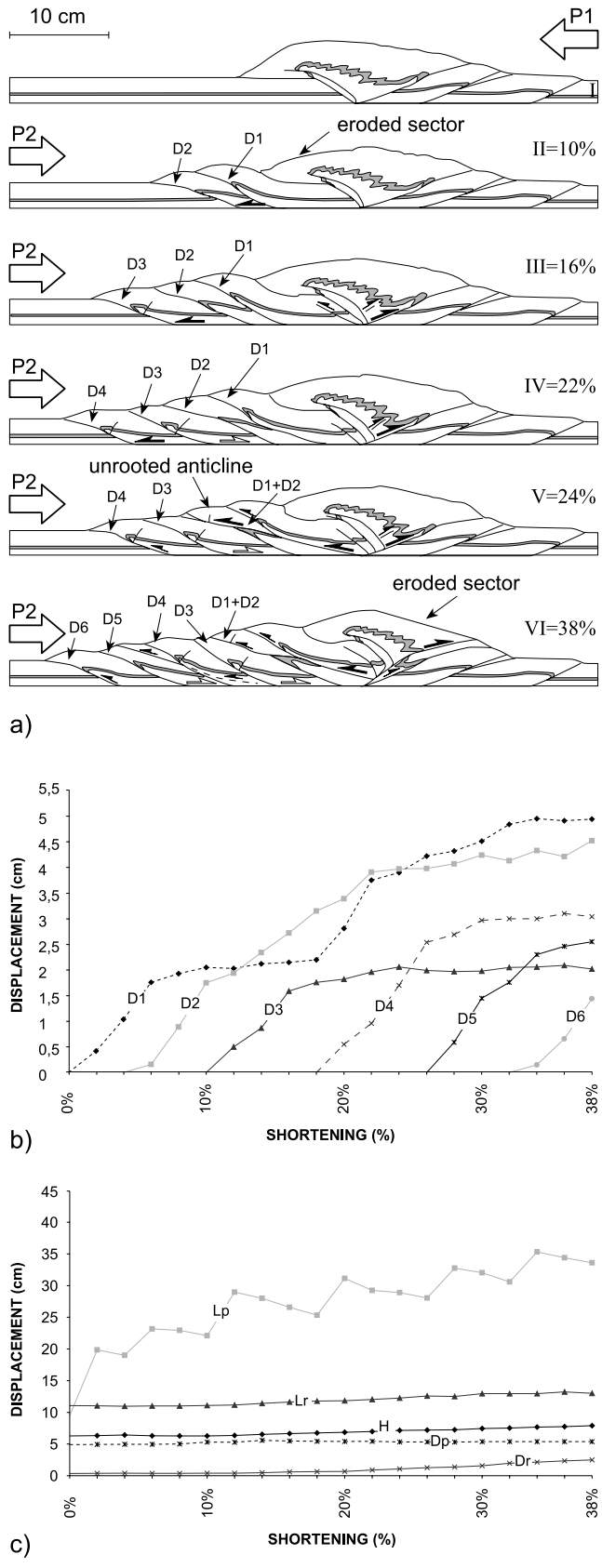

Figure 5. (a) Line drawings of sequential stages of wedge development during the second phase (P2) for experiment CC-38. Stage I is end of the first phase (P1). The white arrows indicate deactivated portions along the basal décollement. In stage VI, the dashed segment denotes initiation of a new underthrusting cycle. (b) Displacement curves with arrangement different from the previous experiment. Stepping up for D1 is evident between 18% and 22% when it finally merges with D2 in a single fault. (c) L_p indicating an initial outward growth for prowedge toe as in CC-36, although less marked. For notation symbols, refer to Figure 4. Because of 100 cm initial undeformed length, percent of shortening equates to centimeters of shortening.

became active, did the prowedge toe start to display its characteristic retreat.

4.4. Kinematics Versus Syntectonic Sedimentation (CC-40)

[22] In the last experiment, the effect of syntectonic sedimentation was analyzed. Instantaneous sedimentary strata were layered in two distinct stages during P2, trying to reproduce a triangular foredeep basin. Layering was scaled to simulate a syntectonic wedge tapering above a basal surface inclined at 3°. As a very first-order approximation, this is intended to represent natural conditions, where the maximum normal stress, therefore maximum confining pressure on potential décollements, is positioned close to the advancing wedge toe. The first layering event added half the thickness of the initial incoming sand section and it was put in before the beginning of P2 (Figure 7a, stage I). At 15% shortening during P2, when a new thrust was about to nucleate, the second, thick sand layer was added. This doubled the incoming section at its point of maximum thickness and covered it over a much wider surface.

[23] At 2% of shortening, a small thrust nucleated beneath the P1 retrowedge region and was offset from the subduction slot (Figure 7a, stage II). As in the other experiments, this event revealed the activation of the P2 retrowedge. At 3% of shortening, a distinct anticline developed at the tip of the detachment propagating at the base of the P2 prowedge (Figure 7a, stage II). The provergent kink band extended up to the syntectonic wedge apex, while the retrovergent kink accommodated an equal amount of displacement, causing a vertical uplift of the anticline. At 15% of contraction, the second syntectonic wedge was added. At this point, the P2 prowedge displayed two long thrust units and an additional ramp starting to deform the sand-pack surface (in cross section a slight bulge in the most external part of the prowedge is visible; Figure 7a, stage III). At the onset of contraction, there was an immediate step back of the active deformation front. At later stages, thrusts in the P2 prowedge were reactivated out of sequence, following a piggyback reactivation sequence, with subsidiary faults branching from main thrusts and shortcutting respective footwalls. At this stage, competition between retrothrust and prowedge basal décollement mutual shear resistances controlled mass transfer within the wedge. Despite an active retrothrust, motion along this fault was insufficient. P2

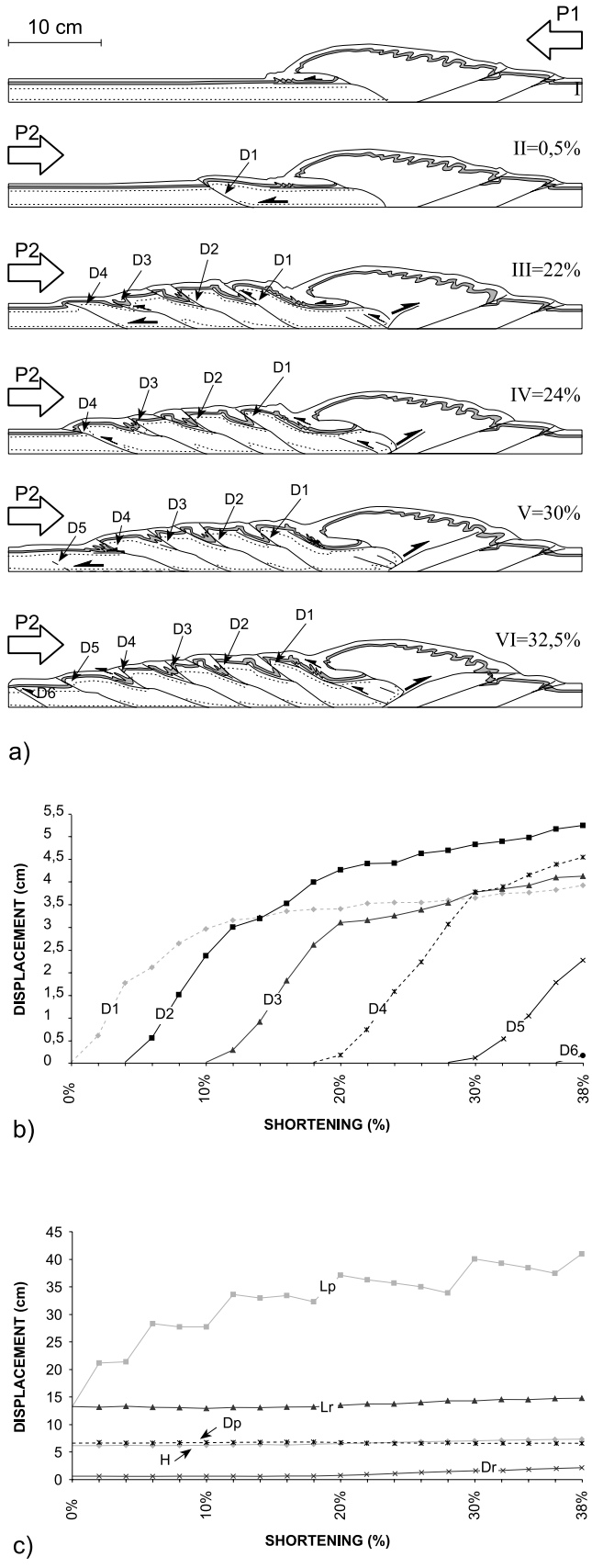

Figure 6. (a) Line drawings of sequential stages of wedge development during the second phase (P2) for experiment CC-39. Stage I is end of the first phase (P1). Small arrows show that some deformation is absorbed along the shallower detachment. (b) Displacement curves denoting simple piggyback nucleation sequence for faults, although cumulative displacement for each of them is very high. (c) Position reached by the prowedge toe (L_p) which is the farthest observed during the experimental program because of a lower basal shear resistance. The positions of the lower and upper glass bead layers are indicated by the dotted horizons. For notation symbols, refer to Figure 4. Because of 100 cm initial undeformed length, percent of shortening equates to centimeters of shortening.

retrowedge became a buttress driving deformation in the P2 innermost prowedge, as confirmed by second-order box folds and related small-scale thrusts at shallow level above the oldest thrust unit in the P2 prowedge (Figure 7a, stage IV). It is at this point that growing stresses at depth overcame the threshold for a new detachment to activate beneath the P2 retrowedge (Figure 7a, stage IV). At 32.5 cm, the P2 prowedge basal detachment finally produced a new ramp, which nucleated well beyond the subduction slot (Figure 7a, stage VI). Surprisingly, it by-passed the preexisting discontinuity positioned where the embryonic thrust had been buried under a thick syntectonic wedge, where shear resistance was assumed to be characterized by a minimum. Toward the end of the model run, the whole wedge (prekinematic plus synkinematic sediments) displayed a superficial taper comparable to CC36 and CC38. However, considering only the prekinematic sand pack, the wedge architecture was highly asymmetric, with a central part "vertically extruded" from the rest of the system.

[24] In this experiment, the displacement curves showed a more irregular shape due to the strong effect of syntectonic sedimentation. Periods of activity along fault surfaces were separated by long quiescence phases. The impact of syntectonic sedimentation is evident from the plot in Figure 7b: (1) the first syntectonic wedge retarded the nucleation of D1; and (2) the second syntectonic wedge prolonged the quiescence phase of D2 and D3, while D1 underwent a marked reactivation. At 24% of contraction, D2 and D3 reactivated simultaneously. At 38% of contraction, D2 had accumulated a total displacement comparable to D2 in CC-39. Most importantly, there was a marked delay in thrust nucleation after the second syntectonic sedimentation event; more than 17% of shortening was necessary before a new anticline transferred the deformation front outward. Another consequence was the distinct reactivation of P2 retrothrust since very early stages of deformation (Figure 7c).

[25] The mechanical link between retrothrust activity and accretion in the prowedge region became evident immediately after the second sedimentation event. At this stage, retrothrust (D_r) underwent a marked increase in displacement rate coupled by rapid P2 retrowedge toe advance (L_r). This increase in retrothrust activity was paralleled, nearly symmetrically, by P2 prowedge retreat (L_p) (the measured prowedge toe position corresponded to the outermost deformation front in the prekinematic sand pack). Yet, a very

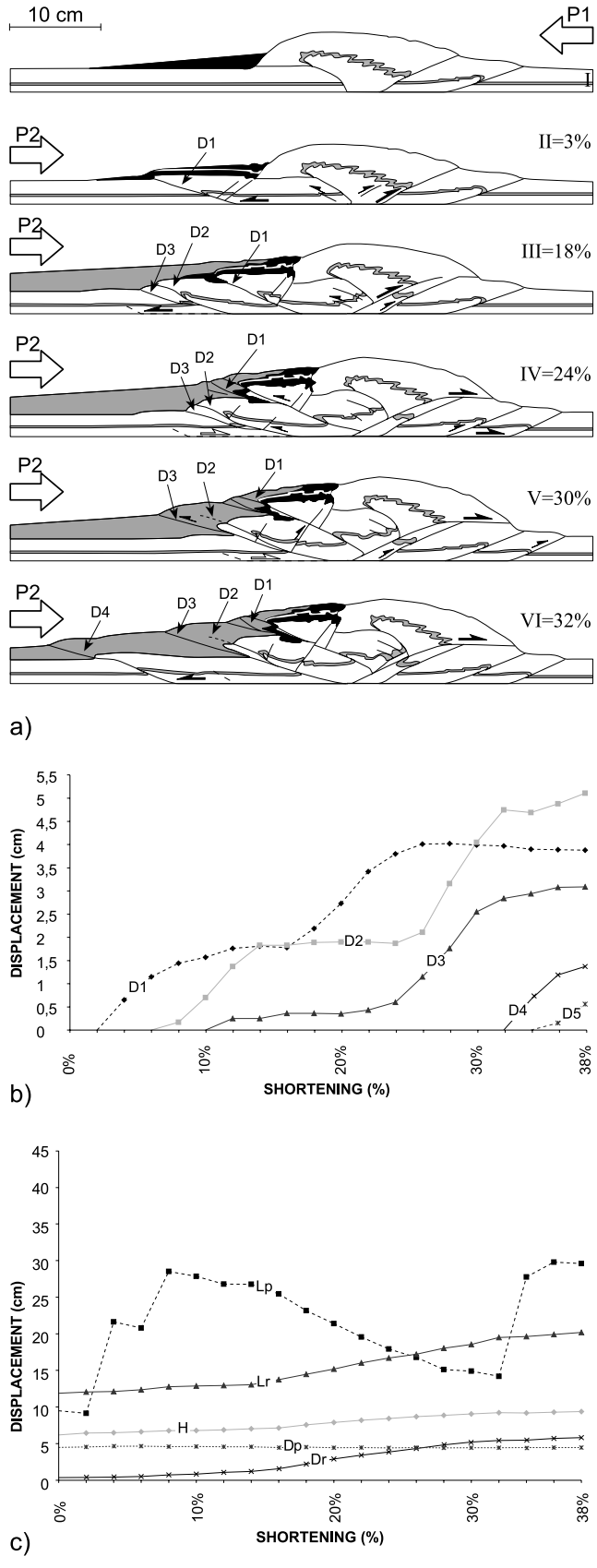

Figure 7. (a) Line drawings of sequential stages of wedge development during the second phase (P2) for experiment CC-40. Stage I is end of the first phase (P1). The white arrows underline the coupling event in the prowedge, accompanied by reactivation of the basal décollement in the retrowedge. (b) Progressive evolution of selected parameters during wedge growth. Note the decreased number of imbricates. (c) Strong variation for D_r, H, and L_r. The prowedge toe clearly retreats (L_p) when the retrothrust activates but nucleation of a new thrust allows a prowedge toe position to be regained comparable to previous experiments. For notation symbols, refer to Figure 4. Because of 100 cm initial undeformed length, percent of shortening equates to centimeters of shortening.

long thrust unit nucleated at 32% of contraction, rebalancing the predicted asymmetric wedge geometry with a prowedge length comparable to other experiments (Figure 7c).

5. Discussion

5.1. Taper Asymmetry

[26] The first remarkable outcome of this experimental program is the asymmetry achieved by the wedge after the subduction polarity reversal. Despite the multiphase deformation applied, each model tended to attain the expected difference in taper between prowedge and retrowedge regions as predicted by theoretical analyses. However, the mechanical equilibrium was approached at different stages during P2 and the relative maximum taper reached by the retrowedge did not show the same value in separate experiments. The mechanical and kinematic aspects of retrowedge growth have already been highlighted [*Koons*, 1990; *Willett et al.*, 1993; *Wang and Davis*, 1996]. In particular, *Wang and Davis* [1996] suggested the existence of a noncritical retrowedge taper in their models and stressed the importance of external factors (such as erosion and/or sedimentation) driving the wedge toward either the end-member states of criticality. Subduction polarity reversal can be seen as one of those factors, for it reverses the P1 prowedge to a final P2 retrowedge location. Because of the drastic "flip" imposed on the contractional system, this experimental procedure tested how the retrowedge responds to renewed stress and velocity boundary conditions, and also whether or not it is capable of keeping its unbalanced state in the retrowedge region for a long deformation interval. Experimental results from this study confirmed *Wang and Davis*' [1996] reasoning that axial zone uplift controls the retrowedge taper growth history. As observed in Figure 8, maximum variations in retrowedge taper ($\Delta\gamma_r$) match the larger variations in axial zone positions between P1 and P2 (ΔH; this would be higher for CC-38 considering the material removed by the denudation events). However, this is not only due to the effect of variable basal friction coefficients in the retrowedge region. Retrowedge slope is also mechanically linked to P2 prowedge growth history, basal décollement activation and taper dynamic variations. All the experiments display similar H_i values at the beginning of P2 and thus, potentially, an equal differential uplift with respect to the axial zone final equilibrium position. Nevertheless, taper increase during P2 varied widely among single experiments. A remarkable difference exists between CC-36 and CC-40. As observed by the differential axial zone uplift (ΔH), CC-40 is characterized by a surplus in vertical motion. This difference was due to the increase in vertical normal stress in P2 prowedge region, related to the syntectonic sedimentary wedge. This pushed P2 prowedge basal décollement within the field of frictional stability for a longer time interval, thereby inhibiting accretion of new imbricates at the prowedge toe and, in turn, provoking active "indentation" of the prowedge region toward the retrowedge region. Accordingly, activity along the retro thrust (ΔD_r) was marked and the retrowedge taper ($\Delta\gamma_r$) was able to grow to a very high value.

[27] Although to a lesser extent, the same difference in retrowedge taper can be observed comparing CC-38 with CC-36. The effect of a syntectonic denudation event on the growing CC-38 P2 prowedge decreased the overall vertical overload within the wedge. The result was a promoted vertical shift of inner thrust units and consequent underthrusting of outer imbricates. This reasoning may explain why retrothrust activity was very low and suggests that the steep slope mainly resulted from retrowedge passive rotation. The effect of prowedge mechanics was confirmed by CC-39. The presence of a more efficient basal detachment promoted only accretion in the P2 prowedge, resulting in minimal P2 retrothrust activity and nearly absent $\Delta\gamma_r$ and ΔH increase.

5.2. Comparison With P1 Kinematics

[28] Wedge growth during P1 was consistent with the kinematics described by *Storti et al.* [2000], in that distinct stages of wedge development were observed. In contrast to *Storti et al.* [2000], no distinct break between the two stages was found in our experiments. An intermediate stage provided a continuous transition, as evinced from the L_p curve in Figure 4e where at about 16% of contraction, the prowedge started to be unstable. This critical point in wedge development was recognized by the formation of small-scale fold at shallow levels in the sand pack stationary region during the P1 phase in CC-39 and a switch from pure uplift to effective wedge backward dislocation was recalled. The nearly linear prowedge toe growth characteristic of early stages of deformation was replaced by a discontinuous trend, whereby every thrust nucleation was followed by a short phase of prowedge toe retreat. Therefore this transitional stage shared common features with the previous one (a reduced prowedge toe propagation) and subsequent stage (a prowedge toe retreat).

[29] As observed in our experiments, there is a substantial difference in the way shortening affected mass transfer during P2. Although varying between different models, activity along single thrust ramps always appeared more long-lived than during P1. Cumulative displacements were indeed much higher (compare displacement curves in Figure 4e with similar ones computed for P2) and the simple piggyback thrust sequence characteristic of the P1 prowedge was substituted by complex deformation paths for material being dragged toward the subduction slot. All these features must be encompassed in the overall behavior shown by the wedge during P2, i.e., a higher rate of prowedge lateral growth. The presence within the wedge of preexisting topography drives accretion of long frontal units at the toe of the P2 prowedge. In other words, the first stage of deformation characteristic of the uplifting axial zone is minimal during P2. For this reason, most of the shortening is absorbed within the P2 prowedge region and the wedge itself grows laterally faster than during P1. Furthermore, the changed stress boundary conditions after the subduction flip require the P1 inherited slope to be lowered, because it is too steep within the new P2 prowedge context. In order to achieve a homogeneous minimum critical taper predicted by theory, the P2 prowedge works in different directions at the same time: (1) accreting material at its toe, therefore building a frontal slope; (2) shifting away the deformation front as far as possible, thus lowering the frontal slope; and (3) uplifting and rotating the region proximal to the P1 retrowedge toe, so its previous maximum taper starts to

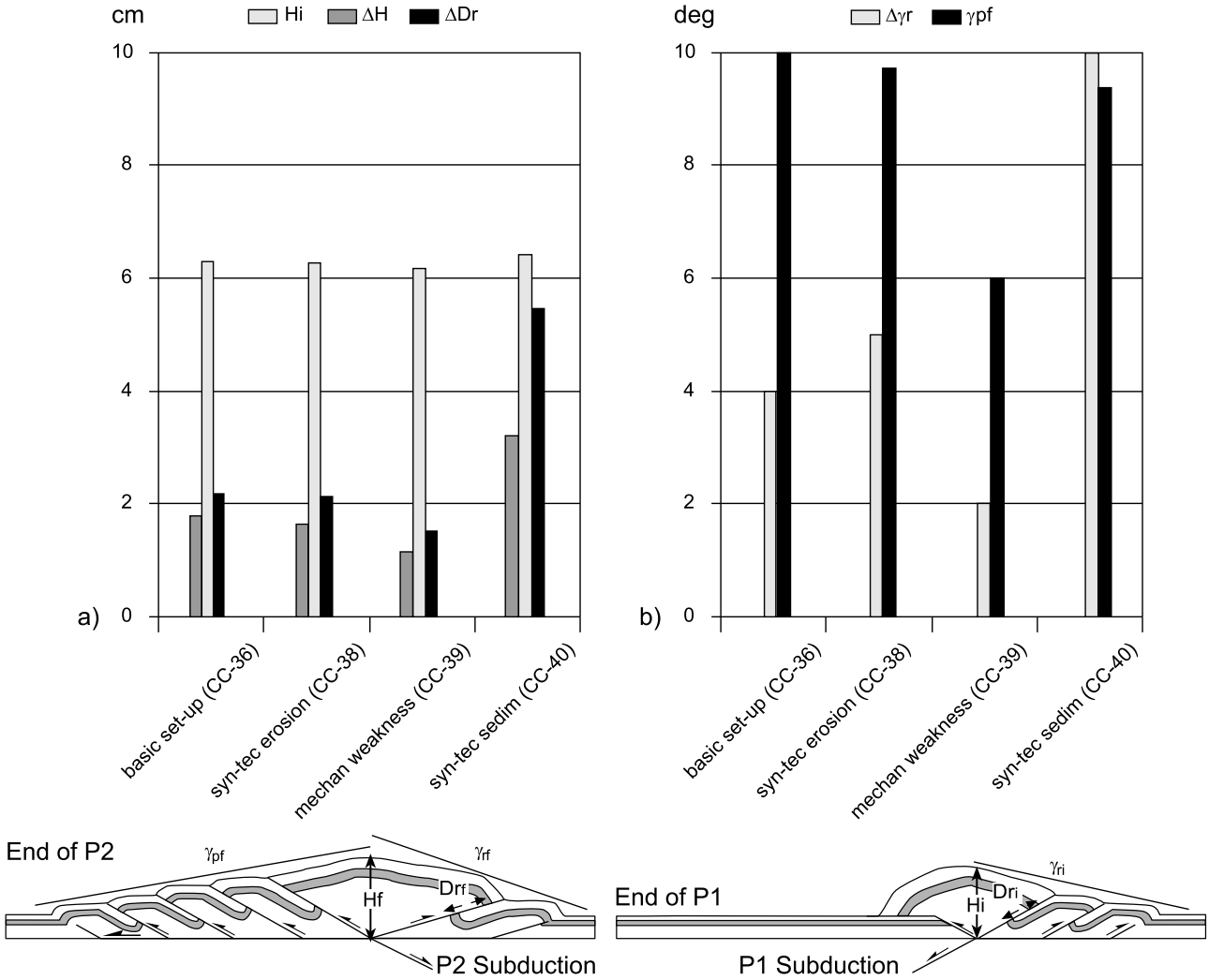

Figure 8. Synoptic plots for this experimental program. (a) Axial zone topography height inherited after the first phase (H_i), differential axial zone height (ΔH), differential retrothrust activity (ΔD_r); (b) differential retrowedge taper ($\Delta\gamma_r$), P2 final prowedge taper (γ_{pf}). These values are expressed as the difference between the end of P1 and end of P2. Axial zone height at the end of the first phase (H_i) is consistent for each experiment. Nevertheless, evolution of selected parameters differs markedly according to various perturbations brought into the accreting system for each experiment (see text for details).

approximate the minimum taper required by mechanical balance for the P2 prowedge.

[30] The stress unbalance left behind in the wedge at the end of P1 controls the mass transfer to fill up the triangular gap existing between the already built up P1 retrowedge region and the flat sand pack (see beginning of P2 shortening for each experiment). This confirms that thrust wedge development is highly sensitive to variations in surface topography [*Marques and Cobbold*, 2002]. Obviously, any perturbation brought into the system can strongly alter the general deformation distribution.

5.3. Accretion Versus Underthrusting

[31] In general, a continuous interplay between accretion at the toe and underthrusting in the innermost part of the prowedge was observed during the experiments. In particular, in CC-36, where the P1 retrowedge region was at its maximum width and was not altered by erosion or sedimentation, the first stage of P2 contraction was marked by continuous accretion of a very short unit at the prowedge toe. This resulted from nearly zero activity along the P2 retrothrust (L_r, Figure 4c), turning the P1 retrowedge region into a vertical, quasi-rigid backstop. For this reason, a secondary strain discontinuity developed away from the subduction slot and persisted for a significant time interval. Only later, with partial activation of the retrothrust, was there distinct out-of-sequence thrusting (synchronous sequence) in the innermost part of the wedge, but in any case underthrusting was very limited. In subsequent experiments, where P1 retrowedge size was kept smaller by a syntectonic denudation event operated on top of it (CC-38), continuous activity of inner thrusts was observed (synchronous thrusting throughout P2 shortening), with clear underthrusting of entire thrust units. From these considerations, one might

conclude that a great overburden (CC-36) is able to stabilize the loaded sedimentary section for a certain time interval, permitting only accretion at the toe. Conversely, a reduced narrower preexisting wedge loading the downgoing sedimentary succession favors underthrusting of material underneath an upward stepping active fault. The same effect might be explained in terms of prowedge transient taper. The CC-36 prowedge displayed a higher taper (P1 retrowedge) than CC-38. In CC-36, progressive rigid rotation of the P1 retrowedge occurred by backthrusting concentrated around the P1 retrowedge toe and out-of-sequence duplexing underneath. This is necessary to the P1 retrowedge to decrease its transient slope down to the minimum taper characteristic of the prowedge. In CC-38, after the first denudation event, the transient taper was already closer to its minimum value, thus a limited rotation was followed by rigid forward displacement that allowed underthrusting of outer imbricates.

[32] Continuous cyclicity between accretion and underthrusting modes has been already described. It was interpreted either as depending upon evolving surface slope of the wedge [*Gutscher et al.*, 1998] or as being controlled by different basal coefficient of friction [*Burbidge and Braun*, 2002]. Our results are consistent with both theories, but the underthrusting/accretion ratio is more limited in our experiments. This might be partly due to a slightly lower basal coefficient of friction than in *Gutscher et al.*'s [1998] experiments. However, the height difference inherited after P1 was much less in the experiments we performed, suggesting that the amount of topography unstable with respect to potential detachments is key to controlling mass transfer modes within a deforming wedge. On the other hand, the interplay between the fixed basal coefficient of friction and the continuous variation of the topographic aspect ratio due to wedge growth and/or the effect of erosional unloading control the dynamic critical stages at which some portions of the basal décollement may be deactivated. This allows transitions to occur locally, from pure frontal accretion to basal underthrusting.

[33] The absence of a slot, in our case, allowing material to exit the system provides a tool for a mass balance condition to be respected so that mass transfer is totally controlled by strain distribution within the wedge. Moreover, no rigid vertical buttress was present in our models. Conversely, the hypothetical output was governed by the activity along the P2 retrothrust, which showed different degrees of displacement and stage of reactivation depending on the variable boundary conditions imposed and/or their dynamic variations them during the course of distinct models. Nevertheless, the similarity of results obtained in distinct experimental procedures is striking. Thus our experiments suggest that the same evolution might also be appropriate for collisional orogens, for which the retrothrust activity is a further control on the balance between accretion and underthrusting modes within the prowedge region.

[34] CC-40 represents an interesting case for different reasons. If the overall wedge aspect (i.e., surface slope and final prowedge toe location) is compared to those of other experiments no major difference emerges. However, in the CC-40 case, the final wedge geometry resulted from a perturbed deformation path, both in terms of timing and mass transfer. At the end of the model run, the syntectonic wedge not being taken into account, a nearly symmetrical, strongly deformed area above the subduction slot can be observed, which is separated by an outer zone where thrust units are very long and nearly flat at depth. The perturbation brought into the system by the addition of the syntectonic wedge might be interpreted in terms of variation of basal shear resistance due to an increase in normal stress acting on the prowedge basal décollement.

[35] Results from finite element analysis [*Willett*, 1999a] suggest that when the basal angle of friction equals the corresponding value characteristic of the deforming material, deformation tends to localize between two major shear zones (prothrust and retrothrust). Accordingly, the wedge grows to its maximum height and assumes a more symmetrical shape. CC-40 showed the same evolution for a significant time interval after the deposition of the second, thicker syntectonic wedge. In this last case though, no variation of basal angle of friction occurs (this is a fixed property for the sand-Mylar film interface), so the sudden increase in normal stress must be evoked as a driving mechanism. This causes transitory coupling of the interface [*Del Castello*, 2003], so that the sand pack can move toward the subduction slot essentially undeformed. The coupling event prolongs the duration and amplifies the velocity contrast between prowedge and retrowedge regions and is responsible, in turn, for persistent deformation in the axial zone, and the highest retrowedge taper measured during the experiments presented here (Figure 8). The renewed frictional stability along the basal décollement prevents absorption of shortening within the prowedge region by accreting new frontal imbricates. At the same time, vertical growth in the axial zone approaches its maximum permitted value. The ''mature'' wedge is thus transported backward as a whole, exerting a push from the rear in P2 retrowedge region. This is sufficient to reactivate the early basal detachment corresponding to the P1 prowedge (Figure 7a, stages IV and V) resembling a phenomenon defined in the past as basal traction reversal [*Willett et al.*, 1993; *Buck and Sokoutis*, 1994].

[36] Transitory coupling also affects deformation timing within the wedge. Nearly 18% of the shortening was absorbed in the inner part of the prowedge before reactivation of the basal décollement. Therefore the time at which thrust units nucleated at the front of the prowedge is markedly different from other experiments, whereas the final overall wedge geometry is very similar. It is worth noting that once propagated, the long detachment at the base of the prowedge did not reactivate a preexisting discontinuity. Conversely, it developed a ramp in such a position as to reequilibrate the prowedge toe location (Figure 7c) predicted by the given value of basal/internal coefficients of friction ratio. This equates to rebalancing the prowedge region minimum critical taper expected after the internal stress reorientation at failure, as in previous experiments (Figure 8).

5.4. A Collisional Perspective

[37] Some considerations on the limitations of the method must be taken into account when trying to interpret natural orogens in the light of these results. These include the impossibility of properly modeling interference between flexure/isostasy and the amount of syntectonic sedimenta-

tion, and the dip of the down going plate (β angle). The first causes an active and continuous variation of the wedge attitude at the surface (α angle). The second alters the rate at which topography is formed, in turn affecting the amount of gravitational unbalance. Therefore topography evolution in laboratory experiments ($\beta = 0$) can only be taken as a gross approximation. As to real cases of collisional systems, both the factors discussed above can be considered to vary in time and space as a composite oceanic-continent transition approaches the collision zone, this being valid for either the prowedge or retrowedge side. As a consequence, the rate at which topography is created can differ, i.e., the effect of an unbalanced internal state of stress might vary in time and in distinct sectors of the orogen itself. For instance, the wedge net elevation is a function of its position with respect to the down going plate curvature [*Bigi et al.*, 2003] and the rheology of the subducting plate [*Wang*, 2001]. The question now arises as to how the wedge dynamically responds to this transition. Is it capable of readjusting rapidly to the change in characteristic variables? Or does the overall wedge aspect derived from early contractional phases interfere with renewed wedge basal conditions such that it strongly affects further deformation? Can unbalanced topography and overload control the rate at which a wedge propagates and also control the vertical evolution of décollement depth in time?

[38] One of the remarkable aspects of wedge growth observed during the experiments performed was the anomalously strong accretionary flux characterizing the P2 prowedge region and the large distance between the subduction slot (strain singularity) and the deformation front from early stages of shortening immediately after the subduction flip event. The extrapolation of these observations to real orogens is not straightforward due to the peculiar dynamic character of accretionary flux [*Gutscher et al.*, 1998; *Burbidge and Braun*, 2002]. In other words, it is not easy to define what stage is reached by an orogen, whether it is still in the accreting mode or underthrusting mode. This is key to our reasoning, as mass transfer modes influence the overall wedge aspect. Thus comparing these laboratory results to nature might be an oversimplification without an in-depth study of the tectonostratigraphic signal, whereby detecting a subduction polarity reversal event by means of a sudden increase in the accretionary flux restricted to well-defined time intervals during such complex tectonic evolutions and positioned at large distances from the supposed location of the plate margin. However, it seems that where subduction polarity reversal is currently active, strong deformation has been detected within the upper plate, far away from the subduction margin, as in the Banda Arc [*Snyder et al.*, 1996]. The same scenario might be envisaged for the northwestern sector of South Island, New Zealand. The overriding plate is here dominated by subhorizontal compression [*Reyners et al.*, 1997] and strong exhumation (up to 3000 m) along discrete contractional structures, which affected the upper plate from the late Miocene to early Pliocene [*King and Trasher*, 1992; *Armstrong et al.*, 1998]. In both settings, the phenomenon takes place just where variably thinned continental crust entered the subduction zone. *Reyners et al.* [1997] interpreted this far-field effect as the result of an interplate coupling episode offshore South Island, New Zealand, where a large accretionary wedge has not yet deformed the trench turbidites. It is impossible to predict whether these systems will eventually undergo a complete polarity reversal, but if this does happen, the early deformation should be preserved somewhere in the tectonostratigraphic record. Thus these recently active settings could be compared to ancient collisional systems, and their geometry might help to unravel the complex tectonic history derived from an evoked subduction polarity reversal event.

[39] Collisional orogens such as the Pyrenees-Cantabrian system, the eastern Alps of Europe and the Apennines all suggest strong involvement of the overriding plate during collision, which might be interpreted in terms of different degrees of ablative subduction and/or subduction polarity reversal. The Pyrenean-Cantabrian system displays an along-strike variation of retrowedge region size (Figure 9). If the Iberian plate is supposed to have behaved coherently as the down going plate subducting toward the north, then progressively stronger involvement must be assumed for the upper plate, from the easternmost sectors to the westernmost ones, up to possible subduction polarity reversal in the Cantabrian-Bay of Biscay region [*Alvarez-Marron et al.*, 1997]. As observed from the serial cross sections, the retrowedge region is very narrow in the eastern Pyrenees profile (Figure 9a; 27 km wide for 37 km of shortening [*Beaumont et al.*, 2000]). In the Central Pyrenees profile (Figure 9b) a similar amount of shortening produces a much wider wedge, up to about 100 km if the sub-Pyrenean zone and Landes shoal are included in the computation [*Teixell*, 1998; *Rocher et al.*, 2000]. In the western Pyrenees-Cantabrian region section (Figure 9c), shortening values are more difficult to obtain and the boundary between the prowedge and retrowedge regions is less clearly defined. However, a width of 56 km accounts only for the accretionary wedge developed at the base of the continental slope, without taking into account inner deformed areas, for an overall shortening value that ranges between 35 km [*Alvarez-Marron et al.*, 1997] and 88 km [*Gallastegui et al.*, 2002]. Most importantly, timing of deformation within the retrowedge region for the latter cases is coeval with the main tectonic phases affecting the Pyrenean prowedge region [*Alvarez-Marron et al.*, 1997; *Rocher et al.*, 2000], suggesting that the two phenomena coexisted during the tectonic history of the Pyrenees.

[40] The eastern Alps of Europe also display an exceptionally wide retrowedge region (Figure 10). A deep reflection seismics interpretation [*TRANSALP Working Group*, 2002] shows a thick-skinned thrust belt developed at the southern edge of this collisional system. Also for the eastern Alps, a close correlation between the main tectonic events for the prowedge and retrowedge regions can be detected, at least until the Serravallian-Tortonian times, when tectonic accretion ended for the prowedge side [*Steininger et al.*, 1986; *Schmid et al.*, 1997], but continued for the retrowedge until Messinian-Pliocene. This might indicate that in this case deformation within the retrowedge region was possibly partitioned in time between ablative subduction and the active indentation suggested for the Adriatic plate [*Castellarin et al.*, 2002]. Nevertheless, a strong bending of the Adriatic deep crustal levels toward the subduction zone can be detected from the seismic profile, and the Adriatic lower crust itself becomes part of the orogen crustal roots as predicted by the ablative subduction model. As a result, the

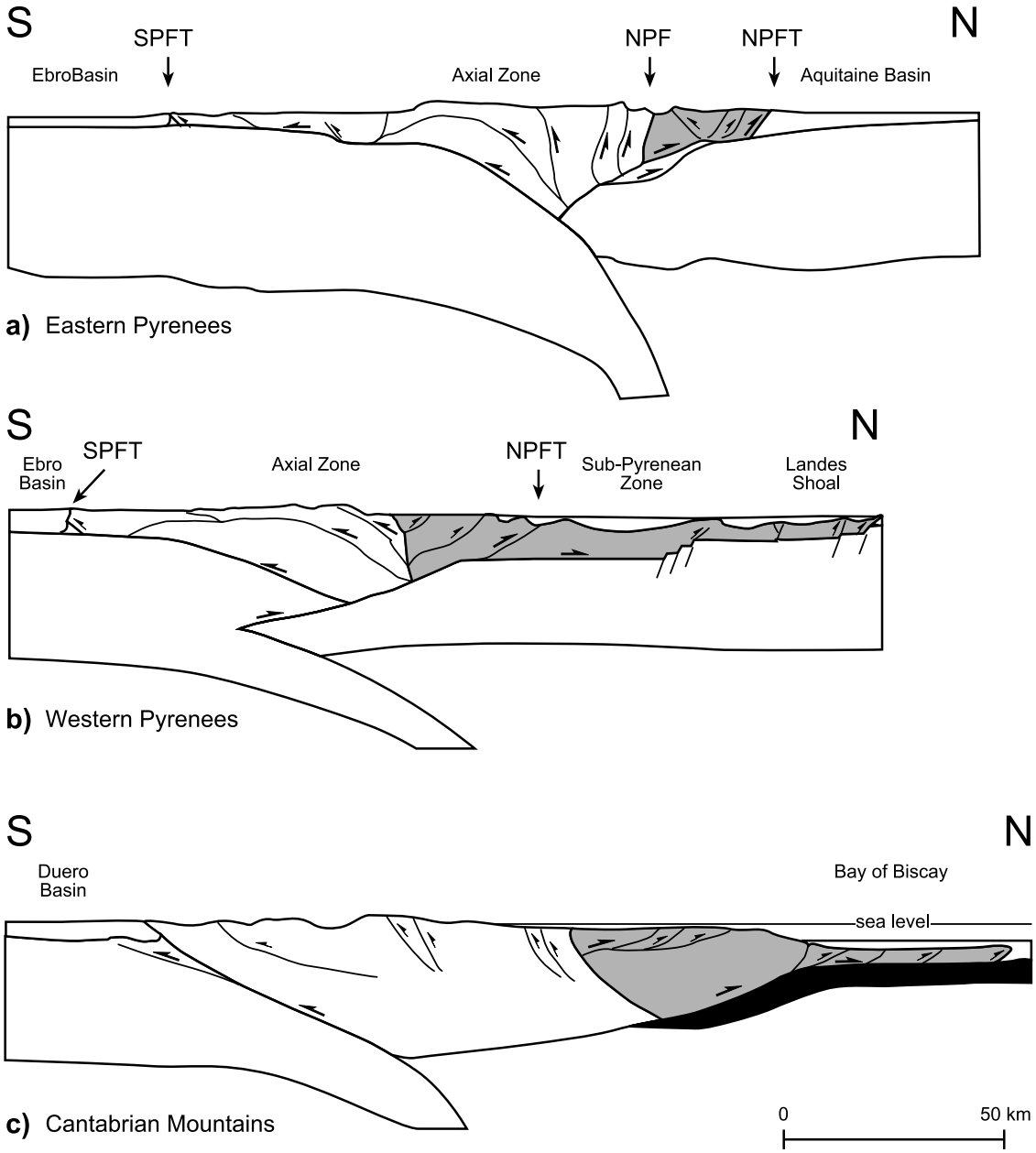

Figure 9. Along-strike variation of the retrowedge region length within the Pyrenees: (a) eastern Pyrenees, (b) western Pyrenees, and (c) Cantabrian Mountains-Bay of Biscay region. Shaded areas indicate the retrowedge region for distinct crustal-scale section, with outer front reconstructed on the basis of coeval deformation phases with the tectonic events within the prowedge region. Black indicates partially subducted oceanic crust in the Bay of Biscay. Data are from *Munoz* [1992] and *Beaumont et al.* [2000] (Figure 9a), *Teixell* [1998] and *Rocher et al.* [2000] (Figure 9b), and *Alvarez-Marron et al.* [1997], *Gallastegui et al.* [2002], and *Pedreira et al.* [2003] (Figure 9c). NPF, North Pyrenean Fault; SPFT, South Pyrenean Frontal Thrust; NPFT, North Pyrenean Frontal Thrust.

uppermost crustal levels are delaminated and accreted in what now appears as a 140 km long retrowedge, for a shortening computed by cross section balancing ranging between 35 km and 40 km only [*Bertelli et al.*, 2002]. Therefore also for this case preexisting topography might have played a role in determining anomalously high accretionary flux within the southeastern Alps.

[41] The Apennines (Italy) could represent the extreme end-member for which a complete subduction flip event occurred for a full continent-continent collision. This fold and thrust system has been interpreted as derived from the Alpine system after a subduction polarity reversal event [*Elter and Marroni*, 1991; *Castellarin*, 1994; *Doglioni et al.*, 1999]. Ablative subduction may be a viable mechanism to explain some discrepancies between the metamorphic and the tectonostratigraphic records of this complex convergent margin soon after the early stages of collision. As for the previous cases, cumulative effects from asymmetric excess topography and vertical overloads acting on the overriding plate may account for the elevated accretionary

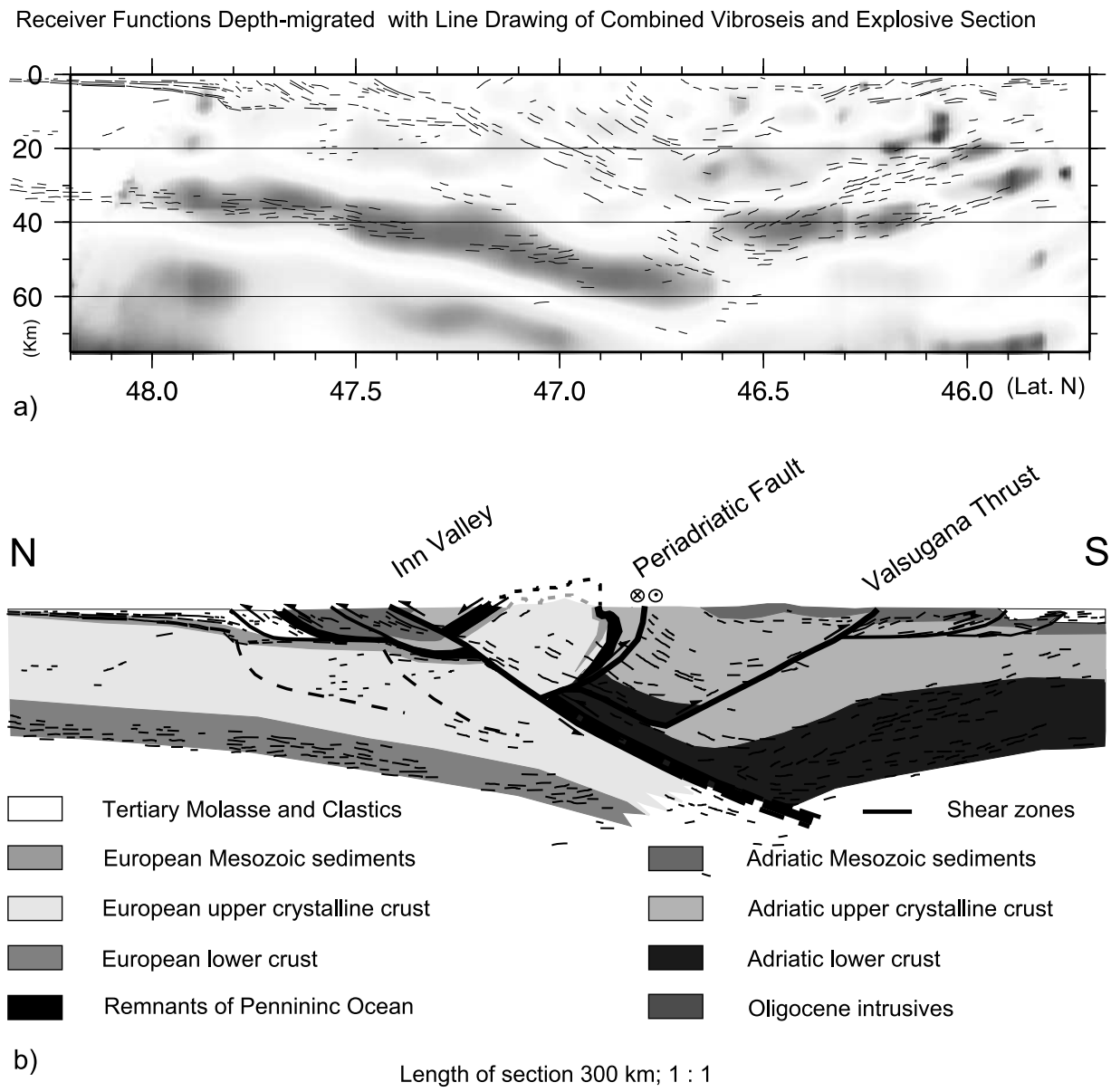

Figure 10. Deep structure of the eastern Alps. (a) Line drawing from Vibroseis and explosive sections superposed onto depth-migrated receiver functions. (b) One interpretation of the geometry of the eastern Alps wedge, obtained by integrating surface and subsurface data. In the retrowedge region, this shows how the upper crust is partially delaminated and involved in the retrowedge structuring; Figure 10b is not to scale. Reprinted from *TRANSALP Working Group* [2002]. See color version of this figure at back of this issue.

flux observed during the early history of Apenninic tectonism. Moreover, the effect of margin-parallel variations of the rheological properties characterizing the crust involved in the deformation may provide an alternative picture to explain some peculiar features concerning the dynamic evolution of the Apenninic orogen [*Del Castello*, 2003].

6. Conclusions

[42] Given the general validity and applicability of the concept of criticality, the balance between wedge bounding surfaces implied in the model remains in equilibrium only in steady state conditions, provided that the basal detachment is everywhere in a state of permanent failure. However, it is important to understand how long a perturbation affecting resistance to traction can be stored within the accreting system before returning to a new equilibrium, and what are the results during this transient stage. This set of experiments illustrates the link between unbalanced topography and dynamic basal shear resistance and how this generates complex mass transfer modes across the wedge. In particular, a fixed critical taper, related to time-invariant frictional properties, is an ideal condition that the wedge is perhaps only able to achieve at a mature stage. Local shear resistance heterogeneities, arising from temporally varying normal stress surpluses and/or from excess topography with respect to existing detachment surfaces can account for the

anomalous behavior of a fold and thrust belt during intermediate stages.

[43] **Acknowledgments.** This work is part of a Ph.D. project granted to M. Del Castello by the University of Bologna, which is acknowledged for funding. M. Del Castello is grateful to P. Whitehouse and T. Dooley at the Fault Dynamics Research Group for their patience while teaching him the sandbox-modeling techniques. Criticism by D. Cowan to an early draft of this paper, and discussion with A. Castellarin were much appreciated. We thank J. Braun, M. A. Gutscher, and an anonymous reviewer. The final version of this paper greatly benefited from their constructive comments.

References

Alvarez-Marron, J., E. Rubio, and M. Torne (1997), Subduction-related structures in the North Iberian Margin, *J. Geophys. Res.*, *102*, 22,497–22,511.

Armstrong, P. A., R. G. Allis, R. H. Funnell, and D. S. Chapman (1998), Late Neogene exhumation patterns in Taranaki Basin (New Zealand): Evidence from offset porosity-depth trends, *J. Geophys. Res.*, *103*, 30,269–30,282.

Beaumont, C., J. A. Munoz, J. Hamilton, and P. Fullsack (2000), Factors controlling the Alpine evolution of the central Pyrenees inferred from a comparison of observations and geodynamical models, *J. Geophys. Res.*, *105*, 8121–8145.

Bertelli, L., L. Cantelli, A. Castellarin, R. Fantoni, A. Mosconi, M. Sella, and L. Selli (2002), Upper crustal style, shortening and deformation ages in the Alps along the southern sector of the TRANSALP profile, in *TRANSALP Conference*, edited by R. Nicolich, D. Polizzi, and S. Furlani, *Mem. Sci. Geol*., Spec. Vol. 54, pp. 127–131, Soc. Coop. Tipogr., Padova, Italy.

Bigi, S., F. Lenci, C. Doglioni, J. C. Moore, E. Carminati, and D. Scrocca (2003), Décollement depth vs accretionary prism dimension in the Apennines and the Barbados, *Tectonics*, *22*(2), 1010, doi:10.1029/2002TC001410.

Braun, J., and C. Beaumont (1995), Three-dimensional numerical experiments of strain partitioning at oblique plate boundaries: Implications for contrasting tectonic styles in the southern Coast Ranges, California, and central South Island, New Zealand, *J. Geophys. Res.*, *100*, 18,059–18,074.

Buck, W. R., and D. Sokoutis (1994), Analogue model of gravitational collapse and surface extension during continental convergence, *Nature*, *369*, 737–740.

Burbidge, D. R., and J. Braun (1998), Analogue models of obliquely convergent continental plate boundaries, *J. Geophys. Res.*, *103*, 15,221–15,237.

Burbidge, D. R., and J. Braun (2002), Numerical models of the evolution of accretionary wedges and fold-and-thrust belts using the distinct-element method, *Geophys. J. Int.*, *148*, 542–561.

Byerlee, J. D. (1978), Friction of rocks, *Pure Appl. Geophys.*, *116*, 615–626.

Carena, S., J. Suppe, and H. Kao (2002), Active detachment of Taiwan illuminated by small earthquakes and its control on first order topography, *Geology*, *30*, 935–938.

Castellarin, A. (1994), Strutturazione eo-mesoalpina dell'Appennino Settentrionale attorno al "nodo ligure", in *Studi Preliminari all'Acquisizione dati del Profilo CROP 1-1A La Spezia-Alpi Orientali*, edited by R. Capozzi and A. Castellarin, *Studi Geol. Camerti*, Vol. Spec. (1992/2 Appendice), pp. 99–108, Univ. di Camerino, Camerino, Italy.

Castellarin, A., G. V. Dal Piaz, R. Fantoni, G. B. Vai, R. Nicolich, and TRANSALP Working Group (2002), Lower crustal style and models along the southern sector of the TRANSALP profile, in *TRANSALP Conference*, edited by R. Nicolich, D. Polizzi, and S. Furlani, *Mem. Sci. Geol.*, Spec. Vol. 54, pp. 245–249.

Chapple, W. M. (1978), Mechanics of thin-skinned fold-and-thrust belts, *Geol. Soc. Am. Bull.*, *89*, 1189–1198.

Chemenda, A. I., R. K. Yang, J. F. Stephan, E. A. Konstantinovskaya, and G. M. Ivanov (2001), New results from physical modelling of arc-continent collision in Taiwan: Evolutionary model, *Tectonophysics*, *333*, 159–178.

Choukroune, P., and The ECORS Team (1989), The ECORS Pyrenean deep seismic profile reflection data and the overall structure of an orogenic belt, *Tectonics*, *8*, 23–39.

Dahlen, F. A. (1984), Non-cohesive critical Coulomb wedges: An exact solution, *J. Geophys. Res.*, *89*, 10,125–10,133.

Daigniéres, M., and The ECORS Team (1994), The Arzacq-western Pyrenees ECORS deep seismic profile, in *Hydrocarbon and Petroleum Geology of France*, *Spec. Publ. Eur. Assoc. Pet. Geosci.*, vol. 4, edited by A. Mascle, pp. 199–208, Springer-Verlag, New York.

DeCelles, P. G., D. M. Robinson, and G. Zandt (2002), Implications of shortening in the Himalayan fold-thrust belt for uplift of the Tibetan Plateau, *Tectonics*, *21*(6), 1062, doi:10.1029/2001TC001322.

Del Castello, M. (2003), Analogue modelling of multiple subduction histories: A case study from the northern Apennines, Ph.D. thesis, 212 pp., Dip. di Sci. della Terra e Geol. Ambientali, Univ. of Bologna, Bologna, Italy.

Doglioni, C., E. Gueguen, P. Harabaglia, and F. Mongelli (1999), On the origin of west directed subduction zones and applications to the western Mediterranean, in *The Mediterranean Basin: Tertiary Extension Within the Alpine Orogen*, edited by B. Durand et al., *Geol. Soc. Spec. Publ.*, *156*, 541–561.

Draper, G., G. Gutiérrez, and J. F. Lewis (1996), Thrust emplacement of the Hispaniola peridotite belt: Orogenic expression of the mid-Cretaceous Caribbean arc polarity reversal?, *Geology*, *24*, 1143–1146.

Elter, P., and M. Marroni (1991), Le unità liguri dell'Appennino Settentrionale: Sintesi dei dati e nuove interpretazioni, *Mem. Desc. Carta Geol. Ital.*, *XLVI*, 121–138.

England, P., and P. Molnar (1997), Active deformation of Asia: From kinematics to dynamics, *Science*, *278*, 647–650.

Gallastegui, J., J. A. Pulgar, and J. Gallart (2002), Initiation of an active margin at the north Iberian continent-ocean transition, *Tectonics*, *21*(4), 1033, doi:10.1029/2001TC901046.

Gutscher, M. A., N. Kukowski, J. Malavieille, and S. Lallemand (1998), Episodic imbricate thrusting and underthrusting: Analog experiments and mechanical analysis applied to the Alaskan accretionary wedge, *J. Geophys. Res.*, *103*, 10,161–10,176.

Hall, R., and M. E. J. Wilson (2000), Neogene sutures in eastern Indonesia, *J. Assoc. Earth Sci.*, *18*, 781–808.

Hodges, K. V., J. M. Hurtado, and K. X. Whipple (2001), Southward extrusion of the Tibetan crust and its effect on Himalayan tectonics, *Tectonics*, *20*, 799–809.

King, P. R., and G. P. Trasher (1992), Post Eocene development of the Taranaki basin, New Zealand: Convergent overprint of a passive margin, in *Geology and Geophysics of Continental Margins*, edited by J. S. Watkins, F. Zhiqiang, and K. J. Millen, *AAPG Mem.*, *53*, 93–118.

Konstantinovskaya, E. A. (2001), Arc-continent collision and subduction reversal in the Cenozoic evolution of the western Pacific: An example from the Kamchatka (NE Russia), *Tectonophysics*, *333*, 75–94.

Koons, P. O. (1990), Two sided orogens: Collision and erosion from sandbox to the Southern Alps, New Zealand, *Geology*, *18*, 679–682.

Lebron, M. C., and M. R. Perfit (1994), Ptreochemistry and tectonic significance of Cretaceous island-arc rocks, Cordillera Oriental, Dominican Republic, *Tectonophysics*, *229*, 69–100.

Liu, H., K. R. McClay, and D. Powell (1992), Physical models of thrust wedges, in *Thrust Tectonics*, edited by K. R. McClay, pp. 71–81, Chapman and Hall, New York.

Malavieille, J. (1984), Modélisation expérimentale des chevauchements imbriqueés: Application aux chaines de montagnes, *Bull. Soc. Geol. Fr.*, *26*, 129–138.

Marques, F. O., and P. R. Cobbold (2002), Topography as a major factor in the development of arcuate thrust belts: Insights from sandbox experiments, *Tectonophysics*, *348*, 247–268.

Marshak, S., and M. S. Wilkerson (1992), Effect of overburden thickness on thrust belt geometry and development, *Tectonics*, *11*, 560–566.

McCaffrey, R. (1992), Oblique plate convergence, slip vectors and forearc deformation, *J. Geophys. Res.*, *97*, 8905–8915.

McClay, K. R. (1990), Deformation mechanisms in analogue models of extensional fault systems, *Deformation Mechanisms, Rheology and Tectonics*, edited by E. H. Rutter and R. J. Knipe, *Geol. Soc. Spec. Publ.* , *54*, 445–453.

Munoz, J. A. (1992), Evolution of a continental collision belt; ECORS-Pyrenees crustal balanced cross-section, in *Thrust Tectonics*, edited by K. McClay, pp. 235–246, Chapman and Hall, New York.

Pedreira, D., J. A. Pulgar, J. Gallart, and J. Díaz (2003), Seismic evidence of Alpine crustal thickening and wedging from the western Pyrenees to the Cantabrian Mountains (north Iberia), *J. Geophys. Res.*, *108*(B4), 2204, doi:10.1029/2001JB001667.

Pfiffner, O. A., S. Ellis, and C. Beaumont (2000), Collision tectonics in the Swiss Alps: Insight from geodynamic modelling, *Tectonics*, *19*, 1065–1094.

Pinet, N., and P. R. Cobbold (1992), Experimental insights into the partitioning of motion within subduction zones, *Tectonophysics*, *206*, 371–388.

Platt, J. P. (1986), Dynamics of orogenic wedges and the uplift of high-pressure metamorphic rocks, *Geol. Soc. Am. Bull.*, *97*, 1037–1053.

Platt, J. P. (1993), Mechanics of oblique convergence, *J. Geophys. Res.*, *98*, 16,239–16,256.

Pope, D. C., and S. D. Willett (1998), Thermal-mechanical model for crustal thickening in the central Andes driven by ablative subduction, *Geology*, *26*, 511–514.

Pulgar, J., and ESCIN Group (1996), Seismic image of the Cantabrian Mountains uplift in the western extension of the Pyrenean Belt from integrated ESCIN reflection and refraction data, *Tectonophysics*, *264*, 1–0.

Reyners, M., R. Robinson, and P. McGinty (1997), Plate coupling in the northern South Island and southernmost North Island, New Zealand, as illuminated earthquake focal mechanisms, *J. Geophys. Res.*, *102*, 15,197–15,210.

Rocher, M., O. Lacombe, J. Angelier, B. Deffontaines, and F. Verdier (2000), Cenozoic folding and faulting in the south Aquitaine Basin (France): Insights from combined structural and paleostress analyses, *J. Struct. Geol.*, *22*, 627–645.

Schellart, W. P. (2000), Shear test results for cohesion and friction coefficients for different granular materials: Scaling implications for their usage in analogue modelling, *Tectonophysics*, *324*, 1–16.

Schmid, S. M., O. A. Pfiffner, N. Froitzheim, G. Schonborn, and E. Kissling (1996), Geophysical-geological transect and tectonic evolution of the Swiss-Italian Alps, *Tectonics*, *15*, 1036–1064.

Schmid, S. M., O. A. Pfiffner, G. Schonborn, and N. Froitzheim (1997), Integrated cross section and tectonic evolution of the Alps along the Eastern Traverse, *Deep Structure of the Swiss Alps*, *Results of NRP 20*, edited by O. A. Pfiffner et al., pp. 289–304, Birkhäuser, Basel.

Smith, C. A., V. B. Sisson, H. G. A. Avé Lallemant, and P. Copeland (1999), Two contrasting pressure-temperature-time paths in the Villa de Cura blueschists belt, Venezuela: Possible evidence for Late Cretaceous initiation of subduction in the Caribbean, *Geol. Soc. Am. Bull.*, *111*, 831–848.

Snyder, D. B., H. Prasetyo, D. J. Blundell, C. J. Pigram, A. J. Barber, A. Richardson, and S. Tjokosaproetro (1996), A dual doubly vergent orogen in the Banda Arc continent-arc collision zone as observed on deep seismic reflection profiles, *Tectonics*, *15*, 34–53.

Steininger, F. F., G. Wesselly, F. Rogl, and L. Wagner (1986), Tertiary sedimentary history and tectonic evolution of the Eastern Alpine Foredeep, *G. Geol.*, *48*, 285–297.

Storti, F., F. Salvini, and K. R. McClay (2000), Velocity-partitioned synchronous thrusting and thrust polarity reversal in experimental doubly vergent thrust wedges accreted at different syntectonic sedimentation rates: Implications for natural orogens, *Tectonics*, *19*, 378–396.

Tang, J. C., and A. I. Chemenda (2000), Numerical modelling of arc-continent collision: Application to Taiwan, *Tectonophysics*, *325*, 23–42.

Tao, W. C., and R. J. O'Connell (1992), Ablative subduction: A two-sided alternative to the conventional subduction model, *J. Geophys. Res.*, *97*, 8877–8904.

Teixell, A. (1998), Crustal structure and orogenic material budget in the west central Pyrenees, *Tectonics*, *17*, 395–406.

TRANSALP Working Group (2002), First deep seismic reflection images of the eastern Alps reveal giant crustal wedges and transcrustal ramps, *Geophys. Res. Lett.*, *29*(10), 1452, doi:10.1029/2002GL014911.

Wang, W. (2001), Lithospheric flexure under a critically tapered mountain belt: A new technique to study the evolution of the Tertiary Taiwan orogeny, *Earth Planet. Sci. Lett.*, *192*, 571–581.

Wang, W., and D. M. Davis (1996), Sandbox model simulation of forearc evolution and noncritical wedges, *J. Geophys. Res.*, *101*, 11,329–11,339.

Willett, S. (1999a), Rheological dependence of extension in wedge models of convergent orogens, *Tectonophysics*, *305*, 419–435.

Willett, S. (1999b), Orogeny and orography: The effects of erosion on the structure of mountain belts, *J. Geophys. Res.*, *104*, 28,957–28,981.

Willett, S., and C. Beaumont (1994), Subduction of Asian lithospheric mantle beneath Tibet inferred from models of continental collision, *Nature*, *369*, 642–645.

Willett, S., C. Beaumont, and P. Fullsack (1993), Mechanical model for the tectonics of doubly vergent compressional orogens, *Geology*, *21*, 371–374.

Wobus, C. W., K. V. Hodges, and K. X. Whipple (2003), Has focused denudation sustained active thrusting at the Himalayan topographic front?, *Geology*, *31*, 861–864.

M. Del Castello, ISMAR-CNR, Sezione di Geologia Marina, Via Gobetti, 101, I-40129, Bologna, Italy. (mario.delcastello@bo.ismar.cnr.it)

K. R. McClay, Fault Dynamics Research Group, Department of Geology, Royal Holloway, University of London, Egham, Surrey, TW20 0EX, UK. (ken@gl.rhul.ac.uk)

G. A. Pini, Dipartimento di Scienze della Terra e Geologico Ambientali, Università di Bologna, Via Zamboni, 67, 40126, Bologna, Italy. (pini@geomin.unibo.it)

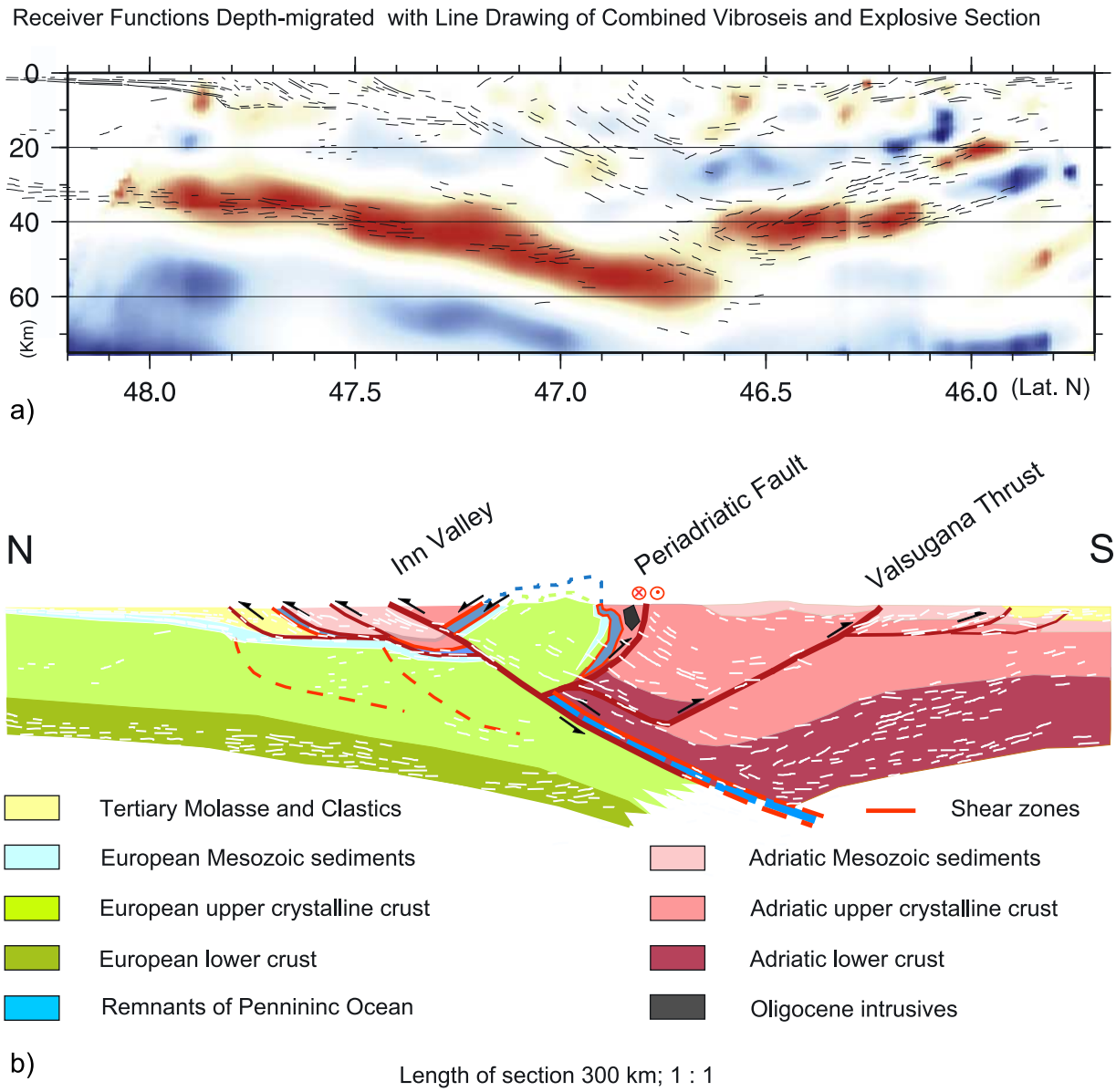

Figure 10. Deep structure of the eastern Alps. (a) Line drawing from Vibroseis and explosive sections superposed onto depth-migrated receiver functions. (b) One interpretation of the geometry of the eastern Alps wedge, obtained by integrating surface and subsurface data. In the retrowedge region, this shows how the upper crust is partially delaminated and involved in the retrowedge structuring; Figure 10b is not to scale. Reprinted from *TRANSALP Working Group* [2002].